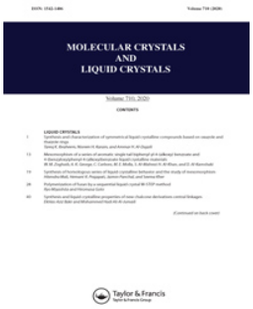

Molecular Crystals and Liquid Crystals

ISSN: (Print) (Online) Journal homepage: https://www.tandfonline.com/loi/gmcl20

Analysis of the dielectric function of aluminum (Al) in bulk and nanometric states

Brahim Ait Hammou, Abdelhamid El Kaaouachi, Abdellatif El Oujdi, Adil Echchelh & Said Dlimi

To cite this article: Brahim Ait Hammou, Abdelhamid El Kaaouachi, Abdellatif El Oujdi, Adil Echchelh & Said Dlimi (2020) Analysis of the dielectric function of aluminum (Al) in bulk and nanometric states, Molecular Crystals and Liquid Crystals, 710:1, 90-102, DOI: 10.1080/15421406.2020.1831726

To link to this article: https://doi.org/10.1080/15421406.2020.1831726

MOLECULAR CRYSTALS AND LIQUID CRYSTALS
2020, VOL. 710, NO. 1, 90–102
https://doi.org/10.1080/15421406.2020.1831726

Analysis of the dielectric function of aluminum (Al) in bulk and nanometric states

Brahim Ait Hammou[a], Abdelhamid El Kaaouachi[a], Abdellatif El Oujdi[b], Adil Echchelh[b], and Said Dlimi[c]

[a]Materials and Physicochemistry of the Atmosphere and Climate Group, Faculty of Sciences of Agadir, Agadir, Morocco; [b]Faculty of Sciences Ibn Tofail, Laboratory of Energetic Engineering and Materials, Kenitra, Morocco; [c]Physics Department, Faculty of Sciences of Agadir, Agadir, Morocco

ABSTRACT

We model the dielectric function of aluminum (Al). The modeling has been performed on Al in bulk and nanometric states. First, we will model the experimental measurements of the dielectric constant as a function of the pulsation ω by appropriate mathematical functions in an explicit way. In the second part, we will highlight the contributions due to intraband and interband electronic transitions. In the last part, we model the dielectric constant of this metal in the nanometric state using several complex theoretical models such as the Drude Lorentz theory and the Drude two-point critical model. We shall comment on which model fits the experimental dielectric function best.

KEYWORDS

Aluminum; bulk; dielectric constant; interband; intraband transitions; IR pulsations; nanometric

1. Introduction

All the intrinsic effects corresponding to the process of light–matter interaction are contained in the dielectric function $\varepsilon(\omega)$. In the case of an isotropic material, the optical response is described by the following equation:

$$\varepsilon(\omega) = \varepsilon_1(\omega) + i\varepsilon_2(\omega), \tag{1}$$

where $\varepsilon(\omega)$ is generally a complex scalar value which depends upon the pulsation ω of the field.

If the medium has an anisotropy, this magnitude is in the form of a tensor. It is often convenient to describe the optical response in an equivalent way from the complex refractive index $\tilde{n} = n + i\kappa$ as n denotes the refractive index describing the phase speed of the wave and κ denotes the extinction index describing the absorption of the wave during propagation in the material. These two indices are directly related to the dielectric constant of the material. In fact, the real and imaginary parts of the dielectric function are deduced from the relation:

$$\varepsilon_1 = n^2 - \kappa^2, \tag{2}$$

CONTACT Brahim Ait Hammou brahim.aithammou1985@gmail.com Materials and Physicochemistry of the Atmosphere and Climate Group, Faculty of Sciences of Agadir, BP 8106, 80000 Agadir, Morocco.

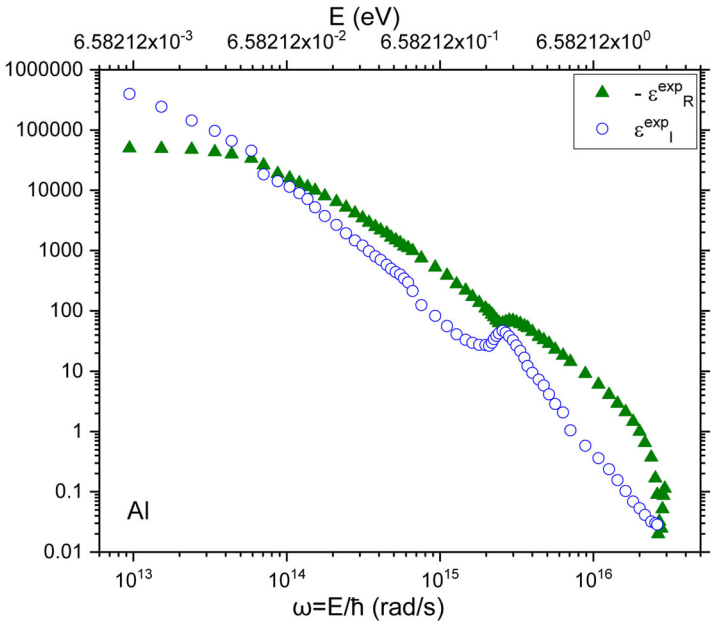

Figure 1. Real part (▲) and imaginary part (*o*) of the dielectric function of bulk Al ([adapted] with permission from [13]).

$$\varepsilon_2 = 2n\kappa, \tag{3}$$

Several important physical quantities can be deduced from the complex refractive index $\tilde{n}$ and dielectric function $\varepsilon(\omega)$ such as the reflectivity coefficient R and the attenuation coefficient α. In the fields of photonics, spintronics, and plasmonics, researchers use the dielectric function in their calculations and investigations [1–8].

2. Modeling of the bulk experimental dielectric function

Here, we try to model the experimental dielectric function $\boldsymbol{\varepsilon^{exp}(\omega)}$ of metal of aluminum (Al) on a wide pulse interval ω with adequate mathematical functions. We consider the measured values of the dielectric function reported by Rakiç et al. [9] in Fig. 1

2.1. Modeling the real part of the bulk experimental dielectric function of Al

In this part, we will model the real and imaginary parts of the experimental dielectric function of Al (Fig. 1). For this, we will divide the values of the pulsation ω into several intervals in order to allow us to determine the best fit to suitable mathematical functions over a certain interval. All the results are presented in Tables 1–10.

For 9.431×10^{12} rad/s $\leq \omega \leq 7.066 \times 10^{13}$ rad/s

$$\varepsilon^{\exp}_{R\_Al}(\omega) = \varepsilon^{0}_{R_0} + \left(2 \times \frac{A}{\pi}\right) \times \left(\frac{B}{4 \times (\omega - \omega_c)^2 + B^2}\right). \tag{4}$$

Table 1. Values of the model parameters.

Parameter	$\varepsilon_{R_0}^0$	A (rad/s)	B (rad/s)	ω_c (rad/s)	R-square (COD)
Value	69013.836	2.281×10^{19}	1.249×10^{14}	1.525×10^{14}	0.9999

Table 2. Values of the model parameters.

Parameter	$\varepsilon_{R_0}^1$	A_1	t_1 (rad/s)	A_2	t_2 (rad/s)	R-square (COD)
Value	477817.293	−31996.297	1.195×10^{14}	−444791.010	1.719×10^{13}	0.99922

Table 3. Values of the model parameters.

Parameter	a_0	a_1 (rad/s)$^{-1}$	a_2 (rad/s)$^{-2}$	a_3 (rad/s)$^{-3}$	a_4 (rad/s)$^{-4}$	R-square (COD)
Value	33370.695	-1.732×10^{-10}	4.029×10^{-25}	-5.362×10^{-40}	4.467×10^{-55}	0.9999
	a_5 (rad/s)$^{-5}$	a_6 (rad/s)$^{-6}$	a_7 (rad/s)$^{-7}$	a_8 (rad/s)$^{-8}$	a_9 (rad/s)$^{-9}$	
	-2.411×10^{-70}	8.444×10^{-86}	-1.852×10^{-101}	2.314×10^{-117}	-1.257×10^{-133}	

Table 4. Values of the model parameters.

Parameter	$\varepsilon_{R_0}^2$	B_1	n_1 (rad/s)	R-square (COD)
Value	3.515	257.945	2.208×10^{15}	0.9993

Table 5. Values of the model parameters.

Parameter	b_0	b_1 (rad/s)$^{-1}$	b_2 (rad/s)$^{-2}$	b_3 (rad/s)$^{-3}$	b_4 (rad/s)$^{-4}$	R-square (COD)
Value	−71346.677	3.014×10^{-15}	-5.608×10^{-27}	6.034×10^{-43}	-4.137×10^{-59}	0.9999
	b_5 (rad/s)$^{-5}$	b_6 (rad/s)$^{-6}$	b_7 (rad/s)$^{-7}$	b_8 (rad/s)$^{-8}$	b_9 (rad/s)$^{-9}$	
	1.875×10^{-75}	-5.618×10^{-92}	1.073×10^{-108}	-1.186×10^{-125}	5.782×10^{-143}	

Table 6. Values of the model parameters.

Parameter	c_0	c_1 (rad/s)$^{-1}$	c_2 (rad/s)$^{-2}$	c_3 (rad/s)$^{-3}$	c_4 (rad/s)$^{-4}$	c_5 (rad/s)$^{-5}$	R-square (COD)
Value	967032.116	-9.199×10^{-8}	4.174×10^{-21}	-9.822×10^{-35}	1.145×10^{-48}	-5.216×10^{-63}	0.9999

Table 7. Values of the model parameters.

Parameter	$\varepsilon_{I_0}^1$	C_1	j_1 (rad/s)	C_2	j_2 (rad/s)	R-square (COD)
Value	1018.824	53821.183	6.302×10^{13}	−127.686	-3.524×10^{14}	0.99922

Table 8. Values of the model parameters.

Parameter	c_0	c_1 (rad/s)$^{-1}$	c_2 (rad/s)$^{-2}$	c_3 (rad/s)$^{-3}$	c_4 (rad/s)$^{-4}$	R-square (COD)
Value	33777.409	-2.016×10^{-10}	5.247×10^{-25}	-7.779×10^{-40}	7.233×10^{-55}	0.9997
	c_5 (rad/s)$^{-5}$	c_6 (rad/s)$^{-6}$	c_7 (rad/s)$^{-7}$	c_8 (rad/s)$^{-8}$	c_9 (rad/s)$^{-9}$	
	-4.377×10^{-70}	1.726×10^{-85}	-4.280×10^{-101}	6.072×10^{-117}	-3.758×10^{-133}	

Table 9. Values of the model parameters.

Parameter	c_0	c_1 (rad/s)$^{-1}$	c_2 (rad/s)$^{-2}$	c_3 (rad/s)$^{-3}$	c_4 (rad/s)$^{-4}$	R-square (COD)
Value	429.849	-2.852×10^{-13}	7.204×10^{-29}	-8.107×10^{-45}	3.410×10^{-61}	0.9982

Table 10. Values of the model parameters.

Parameter	h_0	h_1 (rad/s)$^{-1}$	h_2 (rad/s)$^{-2}$	h_3 (rad/s)$^{-3}$	h_4 (rad/s)$^{-4}$	R-square (COD)
Value	29.949	-1.362×10^{-14}	2.814×10^{-30}	-3.387×10^{-46}	2.600×10^{-62}	0.9999
	h_5 (rad/s)$^{-5}$	h_6 (rad/s)$^{-6}$	h_7 (rad/s)$^{-7}$	h_8 (rad/s)$^{-8}$	h_9 (rad/s)$^{-9}$	
	-1.322×10^{-78}	4.478×10^{-95}	-9.812×10^{-112}	1.271×10^{-128}	-7.454×10^{-146}	

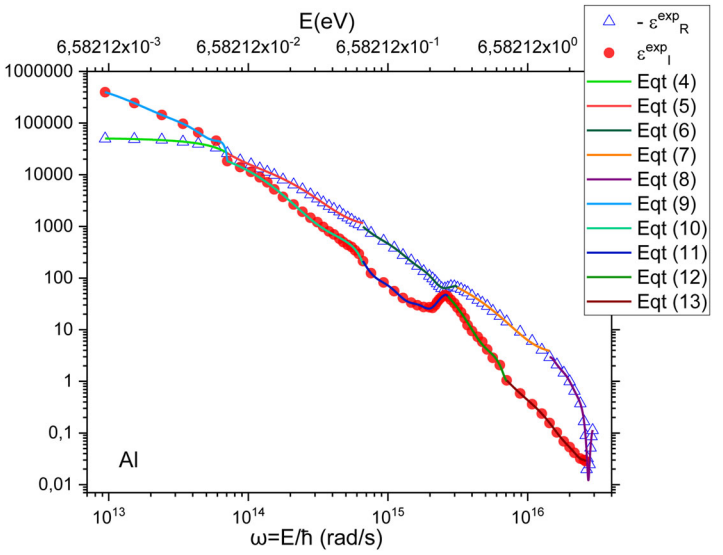

Figure 2. Real (▲) and imaginary (*o*) parts of the experimental dielectric function of bulk Al [13]. Solid colored curves represent, by pulse intervals, the different mathematical models used in the modeling.

For 7.066×10^{13} rad/s $\leq \boldsymbol{\omega} \leq 6.626 \times 10^{14}$ rad/s

$$\varepsilon^{\exp}_{R\_Al}(\omega) = \varepsilon^{1}_{R_0} + A_1\left(1 - e^{-\omega/t_1}\right) + A_2\left(1 - e^{-\omega/t_2}\right). \tag{5}$$

For 6.626×10^{14} rad/s $\leq \boldsymbol{\omega} \leq 3.147 \times 10^{15}$ rad/s

$$\varepsilon^{\exp}_{R\_Al}(\omega) = a_0 + a_1\omega + a_2\omega^2 + a_3\omega^3 + a_4\omega^4 + a_5\omega^5 + a_6\omega^6 + a_7\omega^7 + a_8\omega^8 + a_9\omega^9. \tag{6}$$

For 3.147×10^{15} rad/s $\leq \boldsymbol{\omega} \leq 1.438 \times 10^{16}$ rad/s

$$\varepsilon^{\exp}_{R\_Al}(\omega) = \varepsilon^{2}_{R_0} + B_1 e^{-\omega/n_1}. \tag{7}$$

For 1.438×10^{16} rad/s $\leq \boldsymbol{\omega} \leq 2.925 \times 10^{16}$ rad/s

$$\varepsilon^{\exp}_{R\_Al}(\omega) = b_0 + b_1\omega + b_2\omega^2 + b_3\omega^3 + b_4\omega^4 + b_5\omega^5 + b_6\omega^6 + b_7\omega^7 + b_8\omega^8 + b_9\omega^9. \tag{8}$$

2.2. Modeling the imaginary part of the bulk experimental dielectric function of Al

For 9.431×10^{12}rad/s $\leq \boldsymbol{\omega} \leq 7.066 \times 10^{13}$rad/s

$$\varepsilon^{\exp}_{I\_Al}(\omega) = c_0 + c_1\omega + c_2\omega^2 + c_3\omega^3 + c_4\omega^4 + c_5\omega^5. \tag{9}$$

For 7.066×10^{13}rad/s $\leq \boldsymbol{\omega} \leq 6.626 \times 10^{14}$rad/s

$$\varepsilon^{\exp}_{I\_Al}(\omega) = \varepsilon^{1}_{I_0} + C_1 e^{-\omega/j_1} + C_2 e^{-\omega/j_2}. \tag{10}$$

Table 11. Electronic properties of Al.[a]

Metal	τ (fs)	E (eV)	$\hbar$ (eV s)
Al	11.8	14.98	$6.582119514 \times 10^{-16}$

[a]From Appl. Opt. **37**, 5274 (1998); Appl. Phys. **119**, 085101 (2016).

For $6.626 \times 10^{14}\text{rad/s} \leq \boldsymbol{\omega} \leq 2.681 \times 10^{15}\text{rad/s}$

$$\varepsilon_{I\_Al}^{\exp}(\omega) = c_0 + c_1\omega + c_2\omega^2 + c_3\omega^3 + c_4\omega^4 + c_5\omega^5 + c_6\omega^6 + c_7\omega^7 + c_8\omega^8 + c_9\omega^9. \quad (11)$$

For $2.681 \times 10^{15}\text{rad/s} \leq \omega \leq 7.081 \times 10^{15}\text{rad/s}$

$$\varepsilon_{I\_Al}^{\exp}(\omega) = d_0 + d_1\omega + d_2\omega^2 + d_3\omega^3 + d_4\omega^4. \quad (12)$$

For $7.081 \times 10^{15}\text{rad/s} \leq \omega \leq 2.608 \times 10^{16}\text{rad/s}$

$$\varepsilon_{I\_Al}^{\exp}(\omega) = h_0 + h_1\omega + h_2\omega^2 + h_3\omega^3 + h_4\omega^4 + h_5\omega^5 + h_6\omega^6 + h_7\omega^7 + h_8\omega^8 + h_9\omega^9. \quad (13)$$

All the results of these different models for bulk Al are plotted in Fig. 2.

The experimental results can be well fitted by the models of experimental dielectric function in both its real and imaginary parts with mathematical functions with high accuracy. Indeed, depending on the desired pulse interval, it is possible to use the appropriate mathematical function that best models the experimental values of dielectric function, both in its real and imaginary parts.

3. Highlighting the contribution of interband and intraband transitions in the expression of dielectric function

In metals, there are two types of contribution in the dielectric function, namely contribution of interband transitions denoted by $\varepsilon^{iB}(\omega)$ and that of the intraband transitions denoted by $\varepsilon^{D}(\omega)$. The dielectric function can be written as the sum of two terms

$$\varepsilon(\omega) = \varepsilon^{D}(\omega) + \varepsilon^{iB}(\omega). \quad (14)$$

The first term corresponds to the intraband component of the dielectric constant. It is referred to the optical transitions of a free electron from the conduction band to a higher energy level of the same band. The second term corresponds to the interband component of the dielectric constant. It is referred to optical transitions between the valence bands (mainly d band) and s–p conduction bands. Due to Pauli's exclusion principle, an electron from a valence band can only be excited to the conduction band.

The intraband part $\varepsilon^{D}(\omega)$ of the dielectric function is described by the well-known free electron or Drude Model [10]:

$$\varepsilon^{D}(\omega) = 1 - \frac{\omega_p^2}{\omega(\omega + i\gamma)}, \quad (15)$$

where γ is the collision rate (probability of collision per unit of time).

We note that $\gamma = \tau^{-1}$ and τ is the elastic diffusion time.

In the Drude model, there appears a pulsation called the plasma frequency of a bulk metal given by

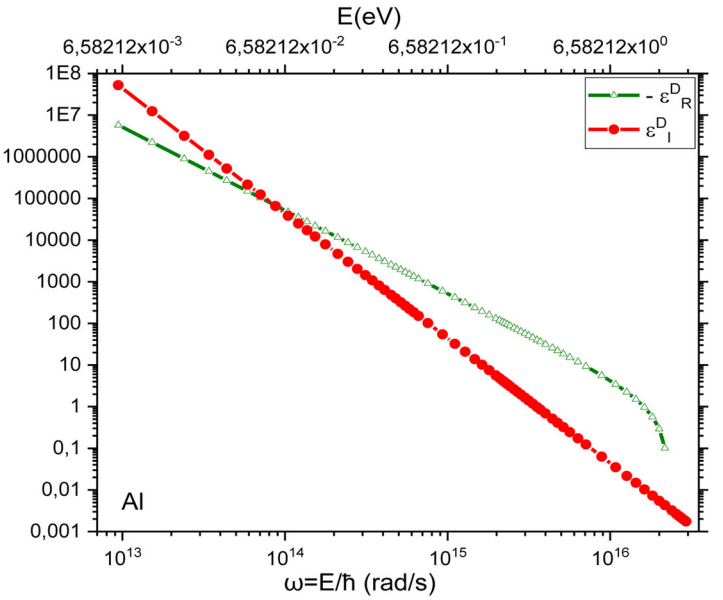

Figure 3. Real (_____ Δ_____) imaginary part (_____ ●_____) of the intraband dielectric function of bulk Al.

$$\omega_p = \frac{E}{\hbar}. \tag{16}$$

The electronic structure of bulk Al, the respective values of the elastic diffusion time τ [11], the plasma frequency E are listed in Table 11.

3.1. Contribution of intraband transitions to dielectric function

The intraband dielectric function described by the Drude model [10] as denoted by $\varepsilon^D(\omega)$ can be written as:

$$\varepsilon^D(\omega) = \varepsilon_R^D(\omega) + i\varepsilon_I^D(\omega). \tag{17}$$

The real and imaginary parts of the relative dielectric function (intraband) are written as follows:

$$\varepsilon_R^D(\omega) = 1 - \frac{\omega_p^2}{\omega^2 + \gamma^2}, \tag{18}$$

$$\varepsilon_I^D(\omega) = \frac{\omega_p^2 \gamma}{\omega(\omega^2 + \gamma^2)}. \tag{19}$$

Usually, for noble metals $\omega \gg \gamma$ in the near UV range and up to the near IR, we can write

$$\varepsilon_R^D(\omega) = 1 - \frac{\omega_p^2}{\omega^2}, \tag{20}$$

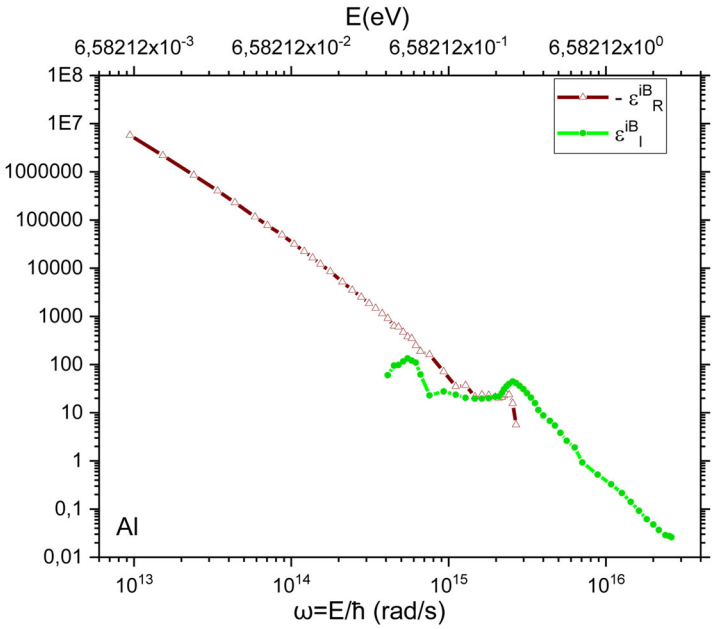

Figure 4. Real (____ Δ____) and imaginary part (____ ●____) of the interband dielectric function of bulk Al.

$$\varepsilon_I^D(\omega) = \frac{\omega_p^2 \gamma}{\omega^3}. \tag{21}$$

The results of the calculations of the contribution of intraband effects to dielectric function are represented in their real and imaginary parts for bulk Al (Fig. 3). The real and imaginary parts decrease by increasing the pulsation. We also note that for $\omega < 0.810^{14}$ rad/s, the real part is smaller than the imaginary part on the other hand for $\omega > 0.810^{14}$ rad/s the real part becomes larger and exceeds the imaginary part.

3.2. Contribution of interband transitions to dielectric function

The interband dielectric function denoted by $\varepsilon^{iB}(\omega)$ is described by the following term:

$$\varepsilon^{iB}(\omega) = \varepsilon_R^{iB}(\omega) + i\varepsilon_I^{iB}(\omega). \tag{22}$$

The real and imaginary parts of the interband dielectric function are written, respectively, as follows:

$$\varepsilon_R^{iB}(\omega) = \varepsilon_R^{\exp}(\omega) - \varepsilon_R^D(\omega), \tag{23}$$

$$\varepsilon_I^{iB}(\omega) = \varepsilon_I^{\exp}(\omega) - \varepsilon_I^D(\omega), \tag{24}$$

where

$$\varepsilon^{\exp}(\omega) = \varepsilon_R^{\exp}(\omega) + i\varepsilon_I^{\exp}(\omega). \tag{25}$$

Here, $\varepsilon^{\exp}(\omega)$, $\varepsilon_R^{\exp}(\omega)$, and $\varepsilon_I^{\exp}(\omega)$ are the experimental values, real and imaginary parts of the complex dielectric function, respectively.

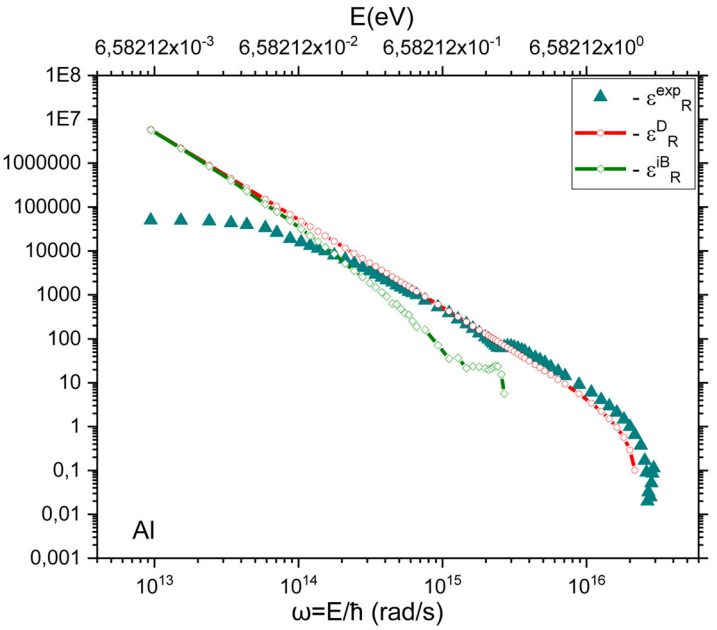

Figure 5. Real parts of the dielectric function of Al: experimental values (▲) [13], intraband transitions (_____o _____), interband transitions (_____ ♦_____).

The results of the calculations of the contribution of interband transitions to real and imaginary parts of dielectric function are represented respectively for bulk Al (Fig. 4)

As shown in Fig. 4, the real and imaginary part of the contribution of interband effects to the dielectric function of bulk Al decrease with increasing pulsation in the IR radiation domain. In Figs. 5 and 6, we have, respectively, presented experimental values, the contributions of intraband and interband transitions to the real and imaginary parts of the dielectric function of Al.

Concerning the real part of the dielectric function, we noted that for $\omega < 1.1 \times 10^{14}$ rad/s, the real parts due to both intraband and interband contributions are practically equal and diverge from the real part of experimental values of the dielectric function. On the other hand, for $\omega > 1.1 \times 10^{14}$ rad/s, we noted that the real part due to the intraband contributions are in perfect agreement with the measured values of the real part of the dielectric function.

Concerning the imaginary part of the dielectric function, we noted that for $\omega > 1.35 \times 10^{14}$ rad/s, the imaginary part due to the interband contributions are practically equal to the imaginary part of the experimental values of the dielectric function. On the other hand, we found that the imaginary part due to the intraband contributions deviates from the experimental values.

4. Modeling the dielectric functions of nanometric Al

In this section, we study the dielectric functions of nanometric Al. They are composed of a few tens to several thousand atoms. Their very small characteristic dimensions, in the nanometer range (*i.e.* well under optical wavelengths), give rise to extraordinary

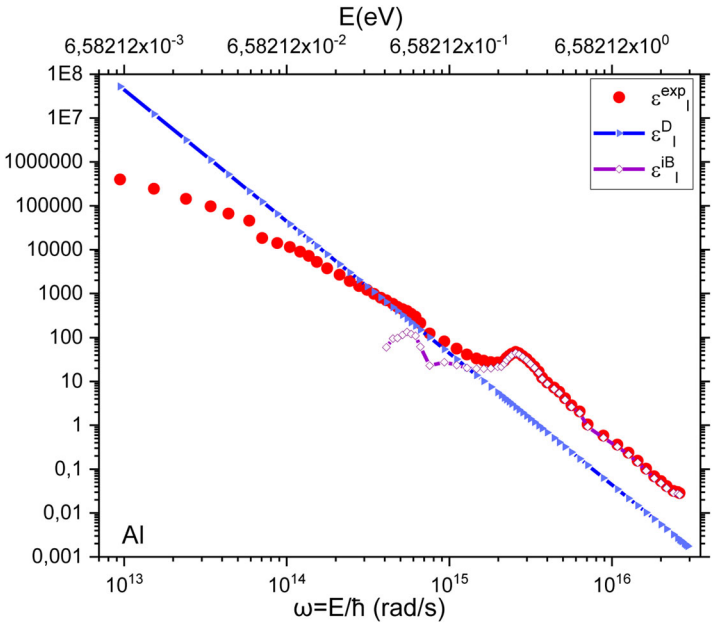

Figure 6. Imaginary parts of the dielectric function of Al: experimental values (●) [13], intraband transitions (____ ▶ ____), interband transitions (____ ♦ ____).

electronic and optical properties that cannot be observed in bulk materials. These properties are clearly influenced by the size, form of the nanoparticle and the nature of the host environment. We consider the measured values of dielectric function used in the previous paragraphs, and try to model those using theoretical models for nanometals such as the Drude–Lorentz (DL) model, and the Drude two-point critical model DCP.

The optical properties of metallic nanoparticles are dominated by the collective oscillation of conduction electrons induced by interaction with electromagnetic radiation (IR, UV). The collective excitation of nanoparticle conduction electrons gives them new optical properties; we consider the following two effects:

- Plasmons guided along a metallic film of nanometric cross-section (1D confinement).
- Surface plasmons located in a metallic particle of nanometric size (0D confinement).

4.1. DL model

For the study of resonant nanostructures, it is important to have a good description of the permittivity of the metal in a large frequency band. For this purpose, the validity band of the Drude Model is often extended by adding Lorentzian terms [12] depending in the following form:

$$\varepsilon_{DL}(\omega) = \varepsilon_{\infty} - \frac{\omega_P^2}{\omega^2 + i\gamma\omega} + \sum_{l=1}^{2} \frac{f_l \Omega_l^2}{\Omega_l^2 - \omega^2 - i\Gamma_l \omega}. \tag{26}$$

Table 12. Optimized parameters of the Drude Lorentz model for Al.[a]

	ε_∞	ω_P (rad/s)	γ (rad/s)	f_1	
Al	2.9649	2.0573×10^{16}	1.2007×10^{14}	8.8701	
	Ω_1 (rad/s)	Γ_1 (rad/s)	f_2	Ω_2 (rad/s)	Γ_2 (rad/s)
Al	2.3743×10^{15}	6.3628×10^{14}	8.6989	3.0074×10^{15}	2.1497×10^{15}

[a]From J. Phys. D. Appl. Phys. **40**, 7154 (2007).

The dielectric function described by the DL model is written as follows:

$$\varepsilon_{DL}(\omega) = \varepsilon_{DL}^{R}(\omega) + i\varepsilon_{DL}^{im}(\omega), \tag{27}$$

where:
The real part of the dielectric function according to the DL model

$$\varepsilon_{DL}^{R}(\omega) = \varepsilon_\infty - \frac{{\omega_P}^2}{\omega^2 + \gamma^2} + \frac{f_1\Omega_1^2(\Omega_1^2 - \omega^2)}{(\Omega_1^2 - \omega^2)^2 + (\Gamma_1\omega)^2} + \frac{f_2\Omega_2^2(\Omega_2^2 - \omega^2)}{(\Omega_2^2 - \omega^2)^2 + (\Gamma_2\omega)^2}. \tag{28}$$

The imaginary part of the dielectric function according to the DL model:

$$\varepsilon_{DL}^{im}(\omega) = \frac{\gamma{\omega_P}^2}{\omega^3 + \gamma^2\omega} + \frac{f_1\Omega_1^2\Gamma_1\omega}{(\Omega_1^2 - \omega^2)^2 + (\Gamma_1\omega)^2} + \frac{f_2\Omega_2^2\Gamma_2\omega}{(\Omega_2^2 - \omega^2)^2 + (\Gamma_2\omega)^2}. \tag{29}$$

The studies of Vial and Laroche [12] on the permittivity of Al metal used in their model with the parameters are listed in Table 12.

The results of modeling the experimental dielectric function in its real and imaginary parts using the DL model are shown in Fig. 7.

4.2. Drude model with two critical points DCP

In order to describe the metal in the largest possible range of pulsations, another formula describing the two-point critical Drude model (DCP) [12] will appear in this paragraph.

The dielectric function of Al can be expressed as [13]:

$$\varepsilon_{DCP}(\omega) = \varepsilon_\infty - \frac{\omega_P^2}{\omega^2 + i\gamma\omega} + \sum_{l=1}^{2} A_l\Omega_l\left[\frac{e^{i\phi}}{\Omega_l - \omega - i\Gamma_l} + \frac{e^{-i\phi}}{\Omega_l + \omega + i\Gamma_l}\right]. \tag{30}$$

The dielectric function described by the Drude two-critical-point model is written as follows:

$$\varepsilon_{DCP}(\omega) = \varepsilon_{DCP}^{R}(\omega) + i\varepsilon_{DCP}^{im}(\omega), \tag{31}$$

where the real part of the dielectric function according to the DCP model:

$$\varepsilon_{DCP}^{R}(\omega) = \varepsilon_\infty - \frac{{\omega_P}^2}{\omega^2 + \gamma^2} + \sum_{l=1}^{2} A_l\Omega_l\left[\frac{(\Omega_l - \omega)\cos\phi_l - \Gamma_l\sin\phi_l}{(\Omega_l - \omega)^2 + \Gamma_l^2} + \frac{(\Omega_l + \omega)\cos\phi_l - \Gamma_l\sin\phi_l}{(\Omega_l + \omega)^2 + {\Gamma_l}^2}\right]. \tag{32}$$

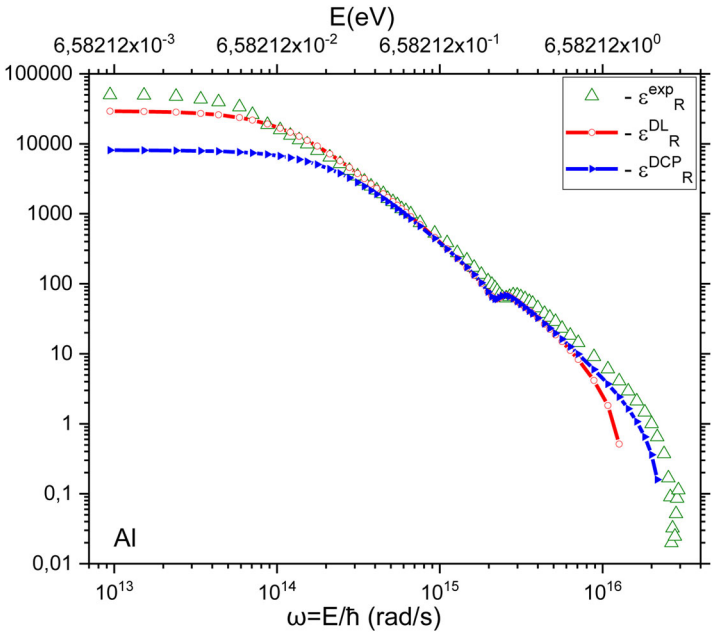

Figure 7. Real part of the dielectric function of nanometric Al: experimental values (Δ) [13], the DL model (——o——) and the DCP model (——▶——).

The imaginary part of the dielectric function according to the DCP model:

$$\varepsilon_{DCP}^{im}(\omega) = \frac{\gamma {\omega_P}^2}{\omega^3 + \gamma^2 \omega} + \sum_{l=1}^{2} A_l \Omega_l \left[\frac{(\Omega_l - \omega)\sin\phi_l + \Gamma_l \cos\phi_l}{(\Omega_l - \omega)^2 + \Gamma_l^2} + \frac{(\Omega_l + \omega)\sin\phi_l - \Gamma_l \cos\phi_l}{(\Omega_l + \omega)^2 + \Gamma_l^2} \right]. \quad (33)$$

The work of Alexandre Vial's [13] on the permittivity of the Aluminum made model with the parameters is listed in Table 13.

The results of modeling the experimental dielectric function in its real and imaginary parts using the Drude two-point DCP critical point model are shown in Fig. 8.

Concerning the real part of the dielectric function, we have noted that for $\omega < 1.2 \times 10^{14}$ rad/s, the real part calculated by using the Drude model is very close to the experimental values. For $1.2 \times 10^{14} < \omega < 1.7 \times 10^{15}$ rad/s, the values calculated by the Drude model and the Drude two-point DCP critical point model are very close to the experimental values with a better results for the Drude two-point DCP critical point model. For $\omega > 1.7 \times 10^{15}$ rad/s, the values of the real part calculated by the Drude model deviate from the experimental values and at the same time the values calculated by the Drude two-point DCP critical point model remain very close to the experimental values.

Concerning the imaginary part of the dielectric function, we have noticed that the imaginary part calculated from the Drude two-point DCP critical point model is in excellent agreement with the experimental values over practically the whole interval of the pulsations. We have also noticed that the values of the imaginary part obtained

Table 13. Optimized parameters of the Drude two-point critical point model DCP, dielectric function for Al.[a]

	ε_∞	ω_P (rad/s)	γ (rad/s)	A_1	ϕ_1 (rad)	Ω_1 (rad/s)
Al	1.0000	2.0598×10^{16}	2.2876×10^{14}	5.2306	−0.51202	2.2694×10^{15}
	A_2	ϕ_2 (rad)	Ω_2 (rad/s)	Γ_2 (rad/s)	Γ_1 (rad/s)	
Al	5.2704	0.42503	2.4668×10^{15}	1.7731×10^{15}	3.2867×10^{14}	

[a]From J. Phys. D. Appl. Phys. **40**, 7154 (2007).

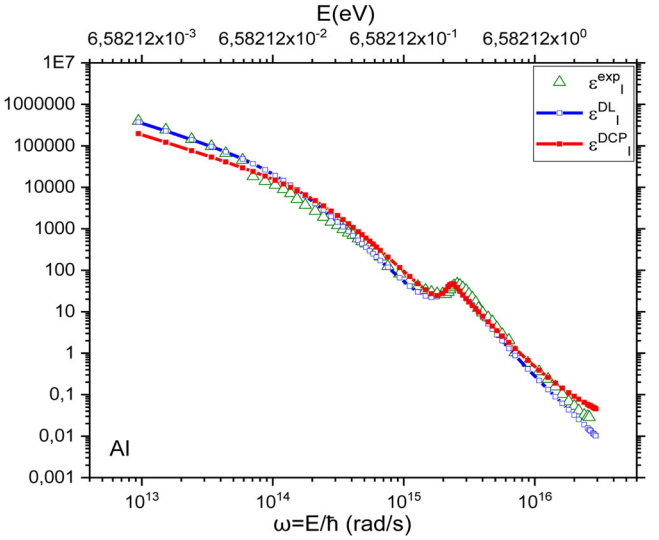

Figure 8. Imaginary part of the dielectric function of nanometric Al: experimental values (Δ) [13], the DL model (——□——) and the DCP model (—— ●——).

using the Drude model are also very close to the experimental values with a slight advantage for the values obtained with the Drude two-point DCP critical point model.

5. Conclusion

In this work, we modeled the dielectric function of Al in its massive and nanometric states. In fact, initially, we modeled the measured dielectric functions of these metal using explicit mathematical functions and in very good agreement with the experiment. Indeed, we have decomposed these measured values of the dielectric function; in its real and imaginary parts; into several intervals according to the pulsations that sweep the domain corresponding to IR radiation. The results obtained are very conclusive, and depending on the pulsation domain studied, it is possible to use the corresponding mathematical function in simulations and calculations. Then, we highlighted the importance of the contributions of intraband and interband transitions in dielectric function for this metal (Al). Concerning the real part of the dielectric function, we noted that for $\omega < 1.1 \times 10^{14}$ rad/s, the real parts due to both intraband and interband contributions are practically equal and diverge from the real part of experimental values of the dielectric function. On the other hand, for $\omega > 1.1 \times 10^{14}$ rad/s, we noted that the real part due to the intraband contributions are in perfect agreement with the measured values of the real part of the dielectric function. Concerning the imaginary part of the dielectric function, we noted that for $\omega > 1.35 \times 10^{14}$ rad/s, the imaginary part due to the interband

contributions are practically equal to the imaginary part of experimental values of the dielectric function. On the other hand, we found that the imaginary part due to the intra-band contributions deviates from experimental values.

Concerning the real part of the dielectric function, we have noted that for $\omega < 1.2 \times 10^{14}$ rad/s, the real part calculated by using the Drude model is very close to the experimental values. For $1.2 \times 10^{14} < \omega < 1.7 \times 10^{15}$ rad/s, the values calculated by the Drude model and the Drude two-point DCP critical point model are very close to the experimental values with a better results for the Drude two-point DCP critical point model. For $\omega > 1.7 \times 10^{15}$ rad/s, the values of the real part calculated by the Drude model deviate from the experimental values and at the same time the values calculated by the Drude two-point DCP critical point model remain very close to the experimental values. Concerning the imaginary part of the dielectric function, we have noticed that the imaginary part calculated from the Drude two-point DCP critical point model is in excellent agreement with the experimental values over practically the whole interval of the pulsations. We have also noticed that the values of the imaginary part obtained using the Drude model are also very close to the experimental values with a slight advantage for the values obtained with the Drude two-point DCP critical point model.

Acknowledgments

We are grateful to Professor Uwe Thumm who hosted us for three months in his James R. Macdonald laboratory at the Kansas State University in the USA, and who offered us an opportunity to collaborate on this subject, as part of the Fulbright Grant Merit Award.

Disclosure statement

The authors declare no conflicts of interest.

References

[1] M. J. Ambrosio and U. Thumm, *Phys. Rev. A* **97** (4), 043431 (2018). doi:10.1103/PhysRevA.97.043431
[2] M. J. Ambrosio and U. Thumm, *Phys. Rev. A* **96** (5), 051403(R) (2017). doi:10.1103/PhysRevA.96.051403
[3] S. R. Leone *et al.*, *Nature Photon.* **8** (3), 162 (2014). doi:10.1038/nphoton.2014.48
[4] F. Calegari *et al.*, *J. Phys. B: At. Mol. Opt. Phys.* **49** (6), 062001 (2016). doi:10.1088/0953-4075/49/6/062001
[5] Y. Li *et al.*, *Opt. Mater. Exp.* **9** (8), 3469 (2019). doi:10.1364/OME.9.003469
[6] M. J. Ambrosio, and U. Thumm, *Phys. Rev. A* **94** (6), 063424 (2016). doi:10.1103/PhysRevA.94.063424
[7] N. Manrique and H. Riascos, Latin America Optics and Photonics Conference, OSA Technical Digest (Optical Society of America, 2018), paper Th4A.16.
[8] F. Roth *et al.*, *J. Electron Spectrosc.* **208**, (2016). doi:10.1016/j.elspec.2015.09.006
[9] A. D. Rakić *et al.*, *Appl. Opt.* **37** (22), 5271 (1998). doi:10.1364/ao.37.005271
[10] C. Kittel, Wiley, New York, 1971.
[11] D. Gall, *J. Appl. Phys.* **119** (8), 085101 (2016). doi:10.1063/1.4942216
[12] A. Vial and T. Laroche, *J. Phys. D: Appl. Phys.* **40** (22), 7152 (2007). doi:10.1088/0022-3727/40/22/043
[13] A. Vial and T. Laroche, *Appl. Phys. B* **93** (1), 139 (2008). doi:10.1007/s00340-008-3202-4